https://doi.org/10.48048/tis.2022.3971

An Automated Framework for Screening of Glaucoma using Cup-to-Disc Ratio and ISNT Rule with a Support Vector Machine

Kay Thwe Min Han[1,*], Pramuk Boonsieng[2], Waree Kongprawechnon[1], Pikul Vejjanugraha[2], Wanicha Ruengkitpinyo[1] and Toshiaki Kondo[1]

[1]*School of Information, Communication and Computer Technologies, Sirindhorn International Institute of Technology, Thammasat University, Pathum Thani 12120, Thailand*
[2]*Faculty of Information Technology, Thai-Nichi Institute of Technology, Bangkok 10250, Thailand*

([*]Corresponding author's e-mail: kthweminhan@gmail.com)

Received: 3 December 2020, Revised: 2 June 2021, Accepted: 9 June 2021

Abstract

Glaucoma is a common eye disease that damages an optic nerve due to abnormally high pressure inside the eye. Glaucoma can cause visual impairments and eventually lead to blindness. There is no appropriate treatment to prevent blindness when the optic nerve is damaged. Therefore, an early diagnosis is important to prevent vision loss from glaucoma. An automated framework for glaucoma screening from fundus images is advantageous. It can facilitate the ophthalmologist in the diagnosis and prevent blindness. Many glaucoma screening algorithms have been developed based on a clinical indicator, the cup-to-disc ratio (CDR). However, these algorithms have some limitations for myopia and genetically large optic cup eyes. Therefore, this paper proposes a framework for glaucoma screening that can be applied even in myopia. The 2 clinical indicators, cup-to-disc ratio (CDR) and neuroretinal rim area rule (inferior > superior > nasal > temporal (ISNT)), are applied in the proposed screening algorithm for accurate glaucoma assessment. Moreover, the automatic classification of glaucoma or non-glaucoma from fundus images is performed by a support vector machine (SVM). Therefore, the experimental results show that the proposed screening algorithm can accurately classify glaucoma to normal eyes or myopic eyes.

Keywords: Glaucoma, Cup-to-disc ratio, ISNT rule, Myopia, Support vector machine

Introduction

Glaucoma is the second leading cause of blindness in the world. According to the first world report on vision issued by the World Health Organization in 2019 [1], the number of people with blindness from glaucoma is estimated at 11.9 million globally. There are various studies on the factors associated with decreasing the risk of developing glaucoma [2-4]. Glaucoma is an eye disease that can cause vision loss by damaging the optic nerve head (ONH) in the eye [5]. Glaucoma is associated with a family history of the disease [5] or with genes related to high eye pressure [6]. Nonetheless, glaucoma can be found at any age [7], but the risk increases in older adults [8,9]. The previous studies have described the impact of glaucoma on the overall health-related quality of life (HRQoL) of patients [10,11], especially in some specific activities such as mobility, reading, and driving [12-16]. In addition, glaucoma has adverse effects on psychological functions such as anxiety, self-image, psychological well-being, and confidence in health care [17].

Glaucoma has no symptoms at the beginning stage and slowly progresses over many years. Therefore, glaucoma is not recognized by many people until the damage is already severe in the ONH [18]. Some people are diagnosed with glaucoma during a routine eye test. Hence, early diagnosis is beneficial for glaucoma patients to save their eyesight. As a result, the patients can be treated early, and vision loss can be prevented. There are several eye tests for glaucoma that can be used by medical doctors or clinicians. Artificial Intelligent (AI) has been used in a variety of approaches to detect, analyze, evaluate, and prognose glaucoma [19]. However, the objective of this paper is to provide automatic glaucoma screening that is less time-consuming, cost-effective, and physician independent. For this reason, the optic nerve head is observed in a fundus image to detect glaucoma. The ONH is composed of

3 main regions which are the optic cup (OC), optic disc (OD), and neuroretinal rim width. **Figure 1** shows the structure of the optic nerve head (ONH).

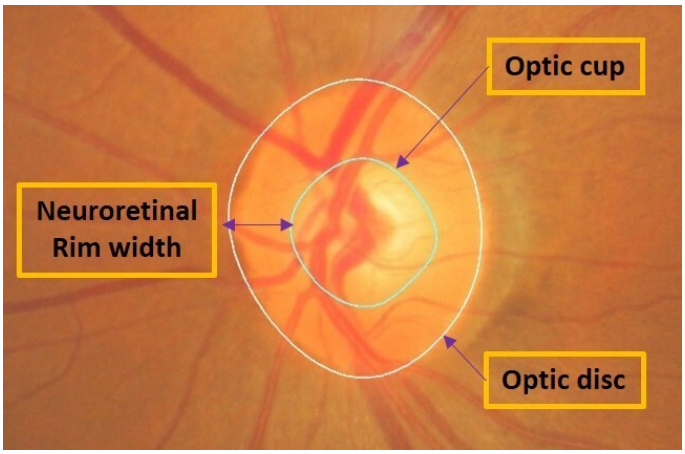

Figure 1 Optic nerve head (ONH).

First, the characteristics of glaucoma are observed. In particular, the optic cup may be expanded due to glaucoma [20]. Hence, the common characteristics of a glaucomatous eye are a larger optic cup than a non-glaucomatous eye. However, some abnormal cases can be found where non-glaucomatous eyes have a larger optic cup than glaucomatous eyes. For example, myopia or nearsighted eyes and genetically large optic cup eyes have large optic cups. In **Figure 2**, a non-glaucomatous ONH with myopia has a large optic cup, compared with a non-glaucomatous ONH without myopia.

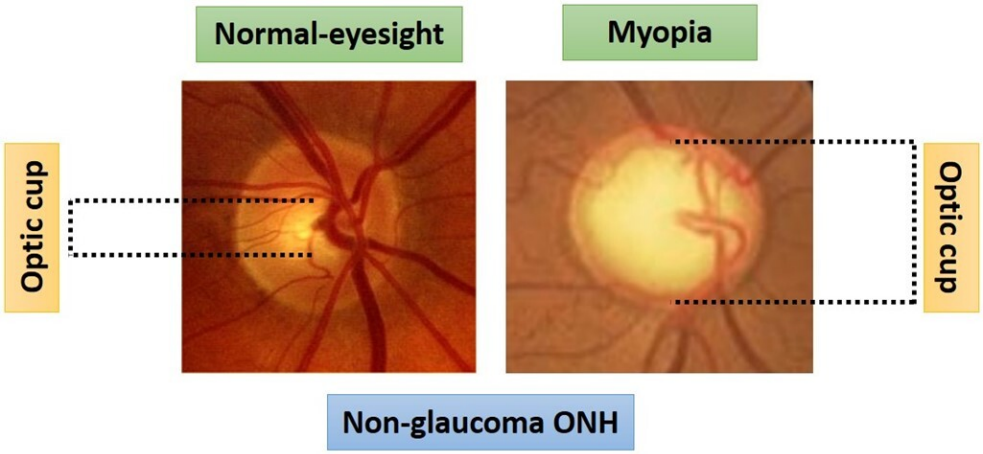

Figure 2 Non-glaucoma ONH: Normal-eyesight eye (left) and myopic eye (right).

Many clinical indicators are employed in automatic glaucoma screening systems. Moreover, special equipment such as an optical coherence tomography camera is also applied in these automatic glaucoma screening systems to generate 3-dimensional eye structures. Consequently, expert ophthalmologists are also required in this kind of system. Overall, these systems demand high expenses for equipment and experts to perform the glaucoma screening.

There are many studies on glaucoma screening algorithms. These algorithms present glaucoma screening with highly efficient results with low expenses [21-27] as the following **Table 1**.

Table 1 Literature review of glaucoma screening algorithms from previous research.

Author	Title	Objective	Methods for glaucoma screening algorithm
Anusorn *et al*., 2013 [21]	Image processing techniques for glaucoma detection using the cup-to-disc ratio	Automatic classification of digital fundus images into either normal or glaucomatous types to facilitate ophthalmologists.	Cup-to-disc ratio (CDR) indicator
Ho *et al*., 2011 [22]	An automatic fundus image analysis system for clinical diagnosis of glaucoma	Glaucoma diagnosis system to calculate automatically and analyze the cup to disc ratio, neuro-retinal rim configuration, abnormal retinal nerve fibers, and the extraordinary retina blood vessels.	CDR indicator and ISNT rims
Narasimhan *et al*., 2012 [24]	Glaucoma detection from fundus image using OpenCV	A semi-automated method for glaucoma detection using CDR and ISNT ratio of a fundus image.	CDR parameters and ISNT rims
Yadav *et al*., 2014 [23]	Classification of glaucoma based on texture features using neural networks	Analysis and diagnosis of the glaucoma from digital fundus images by using image processing technique.	Neural network based on texture features
Wang *et al*., 2014 [25]	Automatic 3D change detection for glaucoma diagnosis	An automatic approach for glaucoma diagnosis based on detecting 3D structure changes in the optic disc area between 2-time sessions.	3D reconstruction
Vejjanugraha *et al*., 2013 [26]	An automatic glaucoma detection method using support vector machine	Automatic screening for glaucoma detection.	CDR indicator and support vector machine (SVM)
Vejjanugraha *et al*., 2017 [27]	An automatic screening method for primary open-angle glaucoma assessment using binary and multi-class support vector machines	An automatic screening technique to diagnose glaucoma by using binary and mult-class support vector machines (SVM).	CDR indicator and support vector machine (SVM)

From the above **Table 1**, CDR and ISNT rims indicators are often applied in the glaucoma screening system. Cup-to-disc ratio (CDR) is defined as the ratio between the diameter of the OC and the OD in vertical and horizontal orientations. However, this indicator is not applicable to myopia and genetically large optic cup eyes due to their large optic cups [28]. Therefore, 1 clinical indicator is not sufficient to detect glaucoma in these special cases [22]. Hence, an additional indicator (ISNT rule) is studied to solve these research issues. In general, a normal optic disk has a neural rim in which the thickness decreases in the order of inferior (I), superior (S), nasal (N), and temporal (T) rims [22,24]. Glaucoma usually affects the superior and inferior optic nerve fibers before the temporal and nasal fibers. Thus, the superior and inferior rims are decreased and the order of ISNT is also changed. The ISNT-rule indicator investigates the neuroretinal rim width in each section of an eye: Inferior (I), superior (S), nasal (N), and temporal (T). Therefore, the ISNT rule can be applied to detect glaucoma for large optic cup cases by determining the neural rim distances for the 4 regions. As a result, glaucoma can be diagnosed at an early stage. In previous glaucoma screening algorithms, one of the clinical indicators, CDR or ISNT is used to examine glaucoma. However, these studies have limitations to classify on myopia or genetically large optic cup. In the proposed screening system, 2 clinical indicators CDR and ISNT are combined to overcome this problem.

Although these 2 clinical indicators can detect glaucoma in the proposed algorithm, an automatic classification is also presented in this paper. For this purpose, a binary classifier called a support vector machine (SVM) is selected. The input features for the SVM are extracted from the CDR and the ISNT rule. Since SVM is used to perform as automatic glaucoma screening algorithm, the proposed screening algorithm can minimize false negative cases and improving an accuracy of a screening system. Therefore, this screening algorithm can identify the glaucoma with either normal size or large size of optic cup.

Moreover, the main contribution of this research is to propose the framework for glaucoma screening by combination of 2 clinical indicators, CDR and ISNT rule in which SVM binary classifier is used to correctly identify glaucoma in fundus images. As a result, this framework can provide less time consuming, cost- effective and physician independent system for glaucoma screening. This paper is organized as follows. The materials and methods are described first, and the automatic glaucoma-screening algorithm is presented. Then, the next section is the results and discussion. The conclusion is in the last section.

Materials and methods

The block diagram of the proposed screening algorithm is depicted in **Figure 3**. Fundus images are used in this algorithm because of their easy accessibility and cost. This type of image can be produced in every hospital at a low cost. Many researchers have utilized fundus images as their inputs [21-24,26,27]. In our framework, input images are first pre-processed by image processing techniques and then a retina analysis step by CDR and ISNT. Finally, SVM is utilized for an automatic classification step.

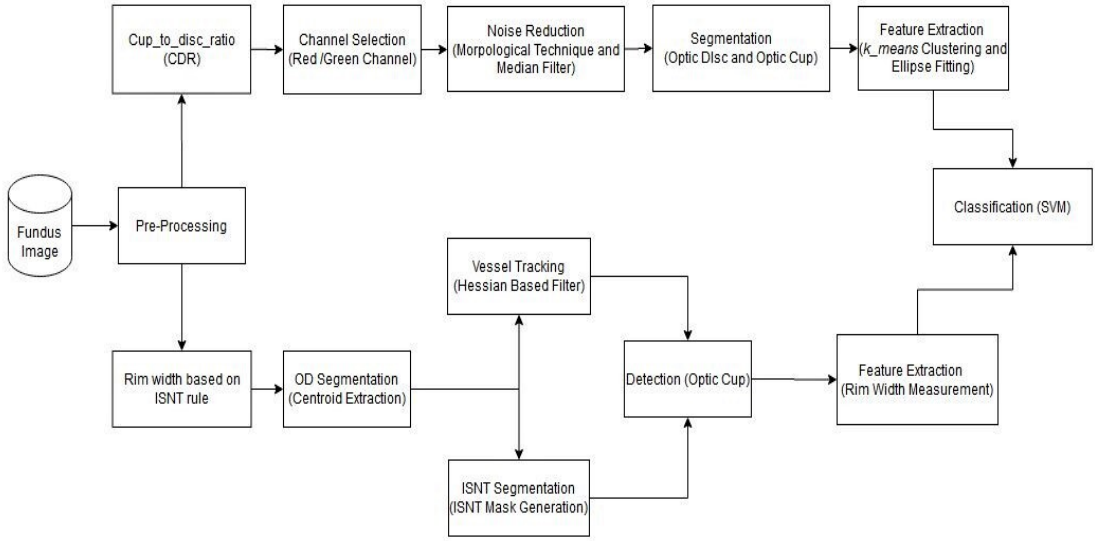

Figure 3 Block diagram of proposed glaucoma screening system.

Pre-processing step

Region of interest (ROI) selection is performed in this pre-processing step. As mentioned earlier, glaucoma can be detected by observing an ONH which is our ROI. However, the interior of a retina is normally present in a fundus image. To reduce the computational cost of the algorithm, an ROI should be correctly selected before proceeding further.

Selecting the ROI can be done by applying the intensity-weighted centroid technique [21]. The centroid of the bright area of a fundus image, which is also the centroid of an ONH, is located by this technique. Afterward, the image is cropped. Only the ROI and its neighboring areas remain.

In this study, all fundus images are obtained from Mettapracharak hospital. Their original size is 2,912×3,166 pixels. After cropping, their new size is 500×500 pixels. These new-size images are called ROI images. ROI images are used as initial images for the subsequent step, retina analysis.

Next, evaluating the glaucoma status of the ROI images is performed as a parallel operation by image processing techniques based on the CDR and the rim width based on ISNT rule. These 2 clinical indicators have been processed for this analysis step, in parallel.

Cup-to-disc ratio (CDR)

The cup-to-disc ratio is the ratio between the size of the optic cup (OC) and the optic disc (OD). It can be calculated by using Eq. (1). Then, the OC and OD of an ROI image need to be segmented.

$$CDR = \frac{Diameter\ of\ the\ optic\ cup}{Diameter\ of\ the\ optic\ disc} \quad (1)$$

Channel selection

Channel selection is performed in this step. Reading the ROI images in color channels is an important step for the OC and OD segmentation. ROI images are RGB images (color images). As a result, they can be read in 3 color channels. Thus, the most suitable color channel should be selected. According to the experiment, the suitable color channels for OC and OD segmentation are the green (G) channel and the red (R) channel, respectively. The output images are called G images and R images according to the reading channel.

Noise reduction

Some noise still exists after reading ROI images in the color channels. In this case, the retinal vessels have noises in the segmentation step [29]. Morphological techniques and a median filter are applied to all R and G images to reduce the noise [26]. A closing operation is performed to remove vessels while the median filter is subsequently executed to smoothen the images.

Segmentation

In this step, optic cup (OC) and optic disc (OD) are segmented. Therefore, a power-law transformation technique is applied for OCs and ODs. The boundaries of the OC and OD are detected by Canny edge detection. It is a Gaussian edge detection in which the performance depends on a Gaussian value. Therefore, Gaussian filter with standard deviation of 1.4 is applied for this segmentation.

Feature extraction

K-means clustering is also applied to select potential candidates for the OC and OD boundaries. However, the shapes of OC and OD are not exactly circular objects. Therefore, ellipse fitting is performed to be a smooth boundary for each OC and OD [21]. Then, diameters of optic cup (DOC) and optic disc (DOD) are measured in both directions in which horizontal diameters are denoted as DOC_H and DOD_H and vertical diameters are referred as DOC_V and DOD_V. All diameter measurements and the CDR calculation are shown in **Figure 4**. Additionally, CDR for both vertical (CDR_V) and horizontal (CDR_H) directions can be calculated based on the Eq. (1) and can be generated as Eqs. (2) - (3);

$$CDR\_H = \frac{DOC\_H}{DOD\_H} \quad (2)$$

where CDR_H = Horizontal cup-to-disc ratio,
DOC_H = Diameter of horizontal optic cup,
DOD_H = Diameter of horizontal optic disc.

$$CDR\_V = \frac{DOC\_V}{DOD\_V} \quad (3)$$

where CDR_V = Vertical cup-to-disc ratio,
DOC_V = Diameter of vertical optic cup,
DOD_V = Diameter of vertical optic disc.

Eventually, features based on the CDR can be extracted. As a result, the extracted features are the diameters of OCs and ODs in a horizontal orientation (DOC_H and DOD_H) and a vertical orientation (DOC_V and DOD_V). Calculated CDR values of the horizontal and vertical orientations (CDR_H and CDR_V) are also used as the features. Moreover, a combination of all horizontal features (Horizontal ALL) and all vertical features (Vertical ALL) give the other 2 features, which can be used as input features for the classification step. Horizontal ALL means combination of DOC_H, DOD _H and CDR_H. On the other hand, Vertical ALL refers to combination of DOC_V, DOD_V, CDR_V). Therefore, a total of 8 input features, based on the CDR indicator, can be extracted in this step. These input features are categorized into 2 feature sets: Horizontal model (DOC_H, DOD_H, CDR_H, and Horizontal ALL) and Vertical model (DOC_V, DOD_V, CDR_V, and Vertical ALL).

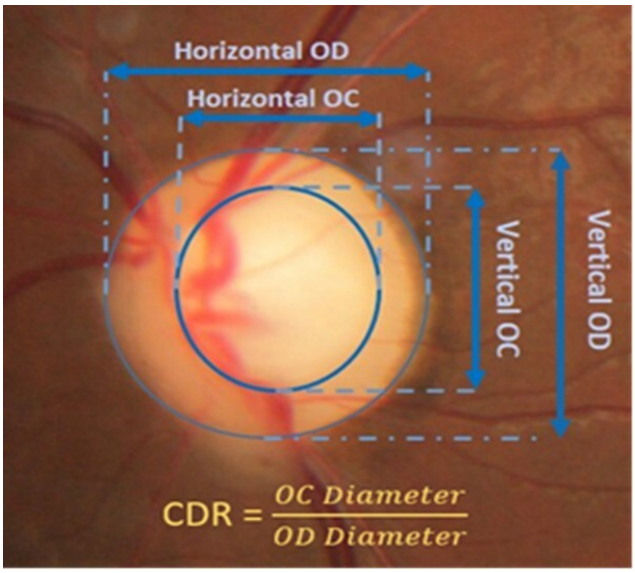

Figure 4 Features based on CDR indicator.

ISNT rule

Another indicator that is utilized for the image analysis process is the ISNT rule. In fact, ISNT refers to the region of the optic nerve which is separated into 4 regions: Inferior (I), superior (S), nasal (N), and temporal (T) rims. Therefore, ISNT rule is defined as the order of the neuroretinal rim width that follows the pattern of I > S > N > T. Firstly, ROI of this indicator is a neuroretinal rim width which can be used for glaucoma screening of myopic ONHs and genetically large ONH. Its ROI is not the same as the CDR indicator. Therefore, a myopic ONH and a genetically large ONH can be analyzed by this indicator without affecting the size of the OC.

OD segmentation

The ROI images are also input images in this step. The centroid of an OD needs to be located because it is important for segmenting the OD into 4 regions: Inferior, superior, nasal, and temporal. This step consists of detection of optic disc (OD) and its centroid. Firstly, ROI images is read in red channel, and it is called R images. Then, R images are converted into binary images which pixels are '1' and background pixels are '0', black. These binary images are called OD binary mages and can be investigated the centroid (Cx; Cy) of the optic disc (white area) for segmentation.

ISNT segmentation

ISNT masks are generated for this ISNT segmentation. Knowing eye anatomy is needed for mask production. The ONH can be divided into 4 regions: Bottommost or inferior (I), uppermost or superior (S), near-nose, or nasal (N), and temporal (T). **Figure 5** shows the isolated regions of an ONH. Utilizing the information of the ISNT regions explained in **Figure 5(a)** with the OD centroid, the mask can be generated [30]. The output masks are called the Inferior mask (I), Superior mask (S), Left-most mask (L), and Right-most mask (R). L and R masks represent nasal and temporal areas, which are different in the left and right eyes, according to **Figure 5(b)**. The side of an eye can be indicated by retinal vessels. More vessels normally appear in the nasal region. Vessel tracking is subsequently processed.

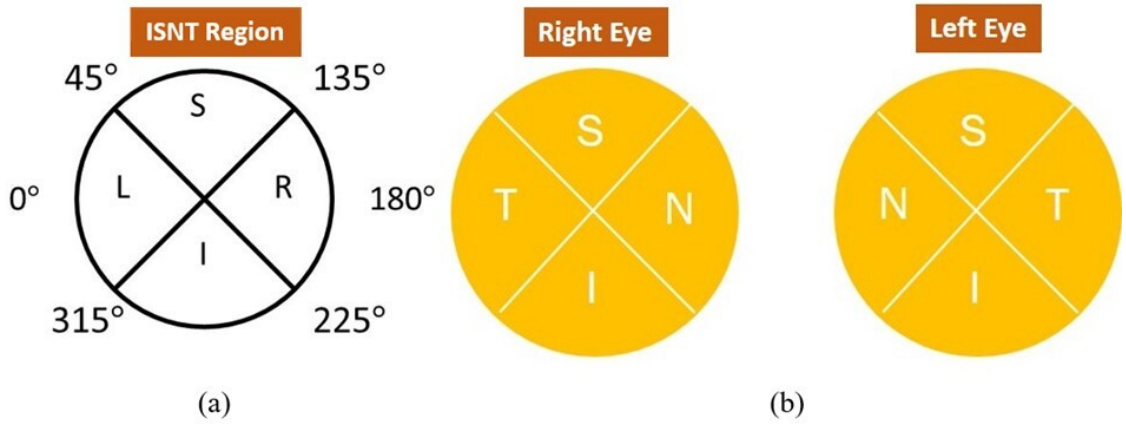

Figure 5 4 regions of ONH (a) ISNT mask region, and (b) ISNT region of the right eye and left.

Vessel tracking

Next, the vessels of interest in the OD region are extracted. Since all the vessels vary in size, multi-scale vessel enhancement is the most suitable technique [31,32]. A frangi filter, a multi-scale vessel enhancement, is applied. This filter is a Hessian-based vessel enhancement. The eigenvalues (λ_1, λ_2) of a Hessian matrix and the principal direction $(\vec{u}_1, \vec{u}_2)$ are calculated from the local second-order structure of the image [33]. This information can be utilized to distinguish vessels from the background [34]. Although a second-derivative filter has more noise sensitivity comparing with a first-derivative filter, it is effective for tracking the center of vessels while the first-derivative filter is suitable for tracking vessel boundaries [35]. For the proposed algorithm, the center lines of vessels are more important than the boundaries since they can be used for OC segmentation.

Optic cup detection

Optic cups can be detected by using retinal vessel bending [32]. Before finding vessel bending points, retinal vessels from the vessel tracking step are isolated into 4 regions, according to the ISNT mask. Then, the number of vessels between the left-most and the right - most regions is compared. Right eyes have more vessels in the rightmost region while left eyes are vice versa. The eye-side, nasal, and temporal regions can be identified in the present stage. Then, the vessel centerline is located by a distance transform technique because its variable size can cause a problem in searching for bending points. After vessel centerlines are created, all candidates of the vessel bending points for each ONH region can be searched. The candidate points are endpoints and junctions of vessels [32]. Bending angles of all candidates are measured afterward. Only vessels that bend into an optic cup are of interest. Thus, the candidates with bending angles of more than 170 °C are eliminated [36]. For enduring candidate points, their bending angles are compared. The points with the highest bending angles in each region are selected to be the OC boundary point for each ONH region.

Feature extraction

The distances between OC boundaries and OD boundaries are called neuroretinal rim widths. Measuring these distances is how features based on ISNT are extracted. **Figure 6** represents a neuroretinal rim width from the algorithm, where the green line is an OD diameter. Also, optic cup boundary points of each region and neuroretinal rim widths are represented by blue stars and black lines, respectively. However, it is difficult to see ONH with a clearly seen bending point in the temporal region (T). Therefore, only the rim width in the inferior (I), superior (S), and nasal (N) regions are used. This feature is called the ISNT rim width (ISNT). Another feature is called the ISNT ratio (ISNT_R), which is composed of I/S, I/N, and S/N. These 3 ratios, I/S, I/N, and S/N should be greater than 1 if an analyzed ONH is non-glaucomatous. The combination of ISNT and ISNT_R is the third feature from the ISNT rule. This last feature is called ISNT ALL.

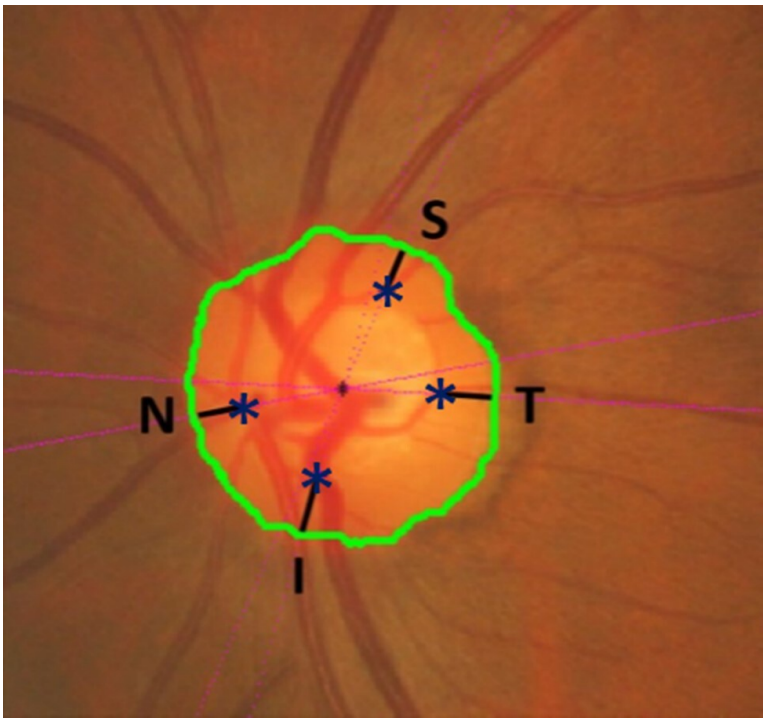

Figure 6 Neuroretinal rim width from the proposed algorithm.

Classification

All extracted features are used as input features for this last step. Four feature models are used in the classification:

Horizontal model: DOC_H, DOD_H, CDR_H, and Horizontal ALL

Vertical model: DOC_V, DOD_V, CDR_V, and Vertical ALL

Rim width model: ISNT, ISNT_R, and ISNT ALL

Combination (proposed) model: Combinations of the best features of each model.

A support vector machine (SVM) is the automatic binary classifier which is applied for this proposed algorithm. In fact, the main purpose of using SVM is to classify a feature in a high dimensional feature space. However, SVM supports different kernel functions which are decision boundaries such as linear, polynomial, and radial basis functions. However, SVM with a linear kernel function is used for the proposed algorithm. Next, features are selected to use the kernel function by finding the optimal hyper plane for separation of the 2 classes: Glaucoma and non-glaucoma. Thus, the input data are isolated into 2 classes. Assigning a target of glaucomatous cases to be 0 while 1 is for the target of non-glaucomatous cases. A 10-fold cross-validation technique is utilized as a generated classifier to examine the data. Therefore, dataset can be divided into 90 % for training set and 10 % for test set. All data are processed by the classifier, based on the input features. These steps are repeated 10 times. Finally, all data are classified.

Results and discussion

A total of 113 fundus images were obtained from Mettapracharak hospital, Thailand. They are categorized based on 2 characteristics: Glaucomatous status and eyesight. By using the glaucomatous status, 54 ONHs are glaucomatous, and the rest are non-glaucomatous ONHs. This data set can also be classified into 15 myopic ONHs and 98 normal-eyesight ONHs by using eyesight as the basis.

The data set is processed through the algorithm with different input features. Then, their performance for screening glaucoma is evaluated by comparing the results with clinical results.

Clinical results

The clinical results (glaucomatous status) are obtained from Mettapracharak hospital. The CDR is the basic indicator for a glaucomatous analysis. An ONH with a CDR value that is greater than 0.65 is classified as a glaucomatous ONH. Otherwise, it is a non-glaucomatous ONH.

Evaluation

The confusion matrix is computed to evaluate the performance of each feature model. Seven indicators are defined in the confusion matrix: True positive (TP), true negative (TN), false positive (FP), false negative (FN), accuracy (ACC), specificity (SPEC), precision (PREC), and sensitivity (SENS).

The TP value is the correctness of glaucomatous indication while the correctness of non-glaucomatous indication is represented by the TN value. In contrast, FP and FN values represent incorrectly identified glaucoma and non-glaucoma, and they are important indicators for this algorithm. Accuracy, specificity, precision, and sensitivity are the correctness percentage of the overall performance, non-glaucomatous indication, and glaucomatous indication. Their calculations are shown in Eqs. (4) - (7);

$$ACC = \frac{TP+TN}{TP+TN+FP+FN} \tag{4}$$

$$SPEC = \frac{TN}{TN+FP} \tag{5}$$

$$PREC = \frac{TP}{TP+FP} \tag{6}$$

$$SENS = \frac{TP}{TP+FN} \tag{7}$$

Cup-to-disc ratio features

The Horizontal and Vertical models are based on the CDR indicator. Four input features of each model are compared. The comparison results among features in both models are summarized in **Tables 2** and **3**. According to **Table 2**, using only the Horizontal CDR(CDR_H) gives the best performance, compared to the other features in the Horizontal model. Likewise, the Vertical CDR(CDR_V) gives the best performance among all features in the Vertical model, as shown in **Table 3**.

Table 2 Comparison among 4 features of the horizontal model.

	Horizontal cup (DOC_H)	**Horizontal disc (DOD_H)**	**Horizontal CDR (CDR_H)**	**Horizontal ALL (DOC_H, DOD_H, CDR_H)**
TP	37	19	**41**	38
TN	45	41	**46**	48
FP	14	18	**13**	11
FN	17	35	**13**	16
ACC	72.6 %	53.1 %	**77.0 %**	76.1 %
SPEC	76.3 %	69.5 %	**78.0 %**	81.4 %
PREC	72.5 %	51.4 %	**75.9 %**	77.6 %
SENS	68.5 %	35.2 %	**75.9 %**	70.4 %

Table 3 Comparison among 4 features of the vertical model.

	Vertical cup (DOC_V)	Vertical Disc (DOD_V)	Vertical CDR (CDR_V)	Vertical ALL (DOC_V, DOD_V, CDR_V)
TP	40	15	**46**	44
TN	45	47	**47**	47
FP	14	12	**12**	12
FN	14	39	**8**	10
ACC	75.2 %	54.9 %	**82.3 %**	80.5 %
SPEC	76.3 %	79.7 %	**79.7 %**	79.7 %
PREC	74.1 %	55.6 %	**79.3 %**	78.6 %
SENS	74.1 %	27.8 %	**85.2 %**	81.5 %

ISNT rule features

The features in the Rim width model are based on the ISNT rule indicator. The same data set is tested with all 3 features in the Rim width model: ISNT, ISNT_R, and ISNT ALL. **Table 4** shows the comparison results of the 3 features. ISNT_R and ISNT ALL give the same performance. However, the ISNT_R feature is chosen as the best feature for the Rim width model because it uses less computational time during reading in the input features.

Table 4 Comparison among 3 features of the rim width model.

	ISNT Rim width (ISNT)	ISNT Ratio (ISNT_R)	ISNT ALL (ISNT, ISNT_R)
TP	44	**48**	48
TN	55	**55**	55
FP	4	**4**	4
FN	10	**6**	6
ACC	87.6 %	**91.2 %**	91.2 %
SPEC	93.2 %	**93.2 %**	93.2 %
PREC	91.7 %	**92.3 %**	92.3 %
SENS	81.5 %	**88.9 %**	88.9 %

Combination (proposed) features

The combination model is an integration of the best features of the other models. **Table 5** shows that a combination of CDR_V and ISNT_R gives the highest accuracy while a combination of CDR_V and CDR_H with ISNT_R has the least false negatives (1 case). If the accuracy is same in 2 model, the less computation time is also considered to choose the best features. Therefore, the best of each model is defined by the most accuracy and less computation time Eventually, a combination of CDR_V and CDR_H with ISNT_R is selected. Although it has slightly less accuracy, false negatives are more important in medical applications.

Table 5 Comparison among 4 features of the combination (proposed) model.

	CDR_V & CDR_H	CDR_V & ISNT_R	CDR_H & ISNT_R	CDR_V & CDR_H & ISNT_R
TP	47	51	48	**53**
TN	47	55	53	**52**
FP	12	4	6	**7**
FN	7	3	6	**1**
ACC	83.2 %	93.8 %	89.4 %	**92.9 %**
SPEC	79.7 %	93.2 %	89.8 %	**88.1 %**
PREC	79.7 %	92.7 %	88.9 %	**88.3 %**
SENS	87.0 %	94.4 %	88.9 %	**98.1 %**

Conclusions

A framework for glaucoma screening has been presented in this study. The objective of this research is to develop an automated framework for glaucoma screening with cost-effective equipment and resources. Since retina fundus images can be found in every hospital, the proposed screening algorithm uses these images due to their easy accessibility and low cost. The second purpose of this paper is the screening algorithm that can assess glaucoma even in the presence of myopia (nearsighted eyes) and a genetically large optic cup ONH. First, the retinal fundus images are captured with an autofocus fundus camera (NIDEK AFC-230) from Mettapracharak Hospital, Nakhon Pathom, Thailand. A total of 113 fundus images are used in the proposed system. Then, 2 clinical indicators, the cup-to-disc ratio (CDR) and the ISNT rule, are applied in the algorithm.

Since CDR is the basic indicator for a glaucoma screening algorithm, many studies have applied this indicator to check the size of an optic cup. However, the large size of the optic cup in myopia cannot be adequately assessed by only this indicator. For this reason, the ISNT rule is applied to detect the ROI of a rim width in each part of an ONH. These 2 indicators are effective in the screening of myopia and a genetically large optic cup (ONH). The proposed algorithm can determine glaucoma for normal and myopic eyesight. The features of glaucoma are extracted by using these 2 indicators and classified by using a support vector machine. From this experiment, a combination of CDR_V and CDR_H with ISNT_R provides the best performance. As a result, this algorithm performs correctly and has found only 1 false negative. Moreover, it also achieves high accuracy, specificity, precision, and sensitivity, which are 92.9, 88.1, 88.3 and 98.1 %, respectively.

This algorithm is written in MATLAB code. Therefore, converting the code into a more general computer language is a future works. Besides, adding more basic indicators could improve the performance of the algorithm. The presence of splinter hemorrhages and displacements of vessels are examples of additional indicators. Moreover, retinal fundus images can also be employed for diabetic retinopathy screening. The proposed glaucoma screening algorithm can be combined with a diabetic retinopathy screening algorithm to examine eye abnormalities.

Acknowledgements

This study was supported by the Center Excellence in Biomedical Engineering of Thammasat University, the Sirindhorn International Institute of Technology (SIIT), Thailand Advance Institute of Science and Technology (TAIST), Tokyo Institute of Technology (Tokyo-Tech), National Science and Technology Development Agency (NSTDA), and National Research University Project (NRU), Thailand Office of Higher Education Commission. Moreover, all medical data and advice are provided by Mettapracharuk (Watraikhing) Hospital and King Chulalongkorn Memorial Hospital.

References

[1] World Health Organization. *Sensory functions and disability and rehabilitation*. World Health Organization, Geneva, Switzerland, 2019.

[2] E Nakano, M Miyake, Y Hosoda, Y Mori, K Suda, T Kameda, HI Ohashi, Y Tabara, K Yamashiro, H Tamura, T Akagi, F Matsuda and A Tsujikawa. Relationship between intraocular pressure and coffee consumption in a Japanese population without glaucoma: The Nagahama study. *Ophthalmol. Glaucoma* 2021; **4**, 268-76.

[3] DA Mammo, M Strampe, A Naravane, PW Mallory, J Boysen and MM Wright. Inpatient adherence to topical glaucoma medications before and after an educational intervention. *Ophthalmol. Glaucoma* 2020; **3**, 339-42.

[4] L Rossetti, M Iester, L Tranchina, L Ottobelli, G Coco, E Calcatelli, C Ancona, P Cirafici and G Manni. Can treatment with citicoline eyedrops reduce progression in glaucoma? The results of a randomized placebo-controlled clinical trial. *J. Glaucoma* 2020; **29**, 513-20.

[5] RN Weinreb, T Aung and FA Medeiros. The pathophysiology and treatment of glaucoma: A review. *J. Am. Med. Assoc*. 2014; **311**, 1901-11.

[6] RS Wang and JL Wiggs. Common and rare genetic risk factors for glaucoma. *Cold Spring Harbour Perspect. Med*. 2014; **4**, a017244.

[7] LP Cohen and LR Pasquale. Clinical characteristics and current treatment of glaucoma. *Cold Spring Harbour Perspect. Med*. 2014; **4**, a017236.

[8] Y Suzuki, A Iwase, M Araie, T Yamamoto, H Abe, S Shirato, Y Kuwayama, HK Mishima, H Shimizu, G Tomita, Y Inoue, Y Kitazawa and the Tajimi Study. Risk factors for open-angle glaucoma in a Japanese population: The Tajimi Study. *Ophthalmology* 2006; **113**, 1613-7.

[9] S Miglior, N Pfeiffer, V Torri, T Zeyen, J Cunha-Vaz, I Adamsons and the European Glaucoma Prevention Study. Predictive factors for open-angle glaucoma among patients with ocular hypertension in the European glaucoma prevention study. *Ophthalmology* 2007; **114**, 3-9.

[10] CEW Chan, PP Chiang, TY Wong, SM Saw, SC Loon, T Aung and E Lamoureux. Impact of glaucoma severity and laterality on vision-specific functioning: The Singapore Malay eye study. *Invest. Ophthalmol. Vis. Sci*. 2013; **54**, 1169-75.

[11] RM Cowdin, Y Wang, J Wu, SP Azen, R Varma and the Los Angeles Latino Eye Study. Impact of visual field loss on health-related quality of life in glaucoma: The Los Angeles Latino eye study. *Ophthalmology* 2008; **115**, 941-8.

[12] SK West, GS Rubin, AT Broman, B Muñoz, K Bandeen-Roche and K Turano. How does visual impairment affect performance on tasks of everyday life? The SEE project. Salisbury eye evaluation. *Arch. Ophthalmol*. 2002; **120**, 774-80.

[13] PY Ramulu, E Maul, C Hochberg, ES Chan, L Ferrucci and DS Friedman. Real-world assessment of physical activity in glaucoma using an accelerometer. *Ophthalmology* 2012; **119**, 1159-66.

[14] C Hochberg, E Maul, ES Chan, SV Landingham, L Ferrucci, DS Friedman and PY Ramulu. Association of vision loss in glaucoma and age-related macular degeneration with IADL disability. *Invest. Ophthalmol. Vis. Sci*. 2012; **53**, 3201-6.

[15] PY Ramulu, BK Swenor, JL Jefferys, DS Friedman and GS Rubin. Difficulty with out-loud and silent reading in glaucoma. *Invest. Ophthalmol. Vis. Sci*. 2013; **54**, 666-72.

[16] PY Ramulu, SK West, B Munoz, HD Jampel and DS Friedman. Driving cessation and driving limitation in glaucoma: The salisbury eye evaluation project. *Ophthalmology* 2009; **116**, 1846-53.

[17] EW Chan, PP Chiang, J Liao, G Rees, TY Wong, JS Lam, T Aung and E Lamoureux. Glaucoma and associated visual acuity and field loss significantly affect glaucoma-specific psychosocial functioning. *Ophthalmology* 2015; **122**, 494-501.

[18] A Septiarini and A Harjoko. Automatic glaucoma detection based on the type of features used: A review. *J. Theor. Appl. Inform. Tech*. 2015; **72**, 368-75.

[19] SK Devalla, Z Liang, TH Pham, C Boote, NG Strouthidis, AH Thiery and MJA Girard. Glaucoma management in the era of artificial intelligence. *Br. J. Ophthalmol*. 2020; **104**, 301-11.

[20] OE Arslan. *Neuroanatomical basis of clinical neurology*. CRC Press, Florida, 2014.

[21] CB Anusorn, W Kongprawechnon, T Kondo, S Sintuwong and K Tungpimolrut. Image processing techniques for glaucoma detection using the cup-to-disc ratio. *Thammasat Int. J. Sci. Tech*. 2013; **18**, 22-34.

[22] C Ho, T Pai, H Chang and H Chen. An automatic fundus image analysis system for clinical diagnosis of glaucoma. *In*: Proceedings of the International Conference on Complex, Intelligent, and Software Intensive Systems, Seoul, Korea. 2011, p. 559-64.

[23] D Yadav, MP Sarathi and MK Dutta. Classification of glaucoma based on texture features using neural networks. *In*: Proceedings of the 7th International Conference on Contemporary Computing, Noida, India. 2014, p. 109-12.
[24] K Narasimhan, K Vijayarekha, KA JogiNarayana, P SivaPrasad and V SatishKumar. Glaucoma detection from fundus image using opencv. *Res. J. Appl. Sci. Eng. Tech*. 2012; **4**, 5459-63.
[25] L Wang, V Kallem, M Bansal, J Eledath, H Sawhney, DJ Pearson and RA Stone. Automatic 3D change detection for glaucoma diagnosis. *In*: Proceedings of the IEEE Winter Conference on Applications of Computer Vision, Colorado, United States. 2014, p. 401-8.
[26] P Vejjanugraha, W Kongprawechnon, T Kondo, S Sintuwong and K Tungpimolkul. An automatic glaucoma detection method using support vector machine. *In*: Proceedings of the SICE Annual Conference, Nagoya, Japan. 2013.
[27] P Vejjanugraha, W Kongprawechnon, T Kondo, K Tungpimolrut and K Kotani. An automatic screening method for primaryopen-angle glaucoma assessment using binary andmulti-class support vector machines. *Sci. Asia* 2017; **43**, 229-39.
[28] M Fingeret. *Cup-to-disc ratio not crucial to glaucoma documentation*. Primary Care Optometry News, New Jersey, 2005.
[29] SS Lee, M Rajeswari, D Ramachandram and B Shaharuddin. Screening of diabetic retinopathy - automatic segmentation of optic disc in colour fundus images. *In*: Proceedings of the 2nd International Conference on Distributed Frameworks for Multimedia Applications, Pulau Pinang, Malaysia. 2006.
[30] S Darsana and RM Nair. Mask image generation for segmenting retinal fundus image features into ISNT quadrants using array centroid method. *Int. J. Res. Mod. Eng. Emerg. Tech*. 2014; **3**, 263-7.
[31] MH Tan, Y Sun, SH Ong, J Liu, M Baskaran, T Aung and TY Wong. Automatic notch detection in retinal images. *In*: Proceedings of the IEEE 10th International Symposium on Biomedical Imaging, California, United States. 2013.
[32] WWK Damon, J Liu, TN Meng, Y Fengshou and WT Yin. Automatic detection of the optic cup using vessel kinking in digital retinal fundus images. *In*: Proceedings of the 9th IEEE International Symposium on Biomedical Imaging, Barcelona, Spain. 2012.
[33] AF Frangi, WJ Niessen, KL Vincken and MA Viergever. Multiscale vessel enhancement filtering. *In*: Proceedings of the Medical Image Computing and Computer-Assisted Intervention, Massachusetts, United States. 1998.
[34] DJ Carretero, A Santos, S Kerkstra, RD Rudyanto and MJL Carbayo. 3D frangi-based lung vessel enhancement filter penalizing airways. *In*: Proceedings of the 2013 IEEE 10th International Symposium on Biomedical Imaging, San Francisco CA, United States. 2013.
[35] K Krissian, J Ellsmere, K Vosburgh, R Kikinis and CF Westin. Multiscale segmentation of the aorta in 3D ultrasound images. *In*: Proceedings of the 25th Annual International Conference of the IEEE Engineering in Medicine and Biology Society, Cancun, Mexico. 2003.
[36] GD Joshi, J Sivaswamy, K Karan, R Prashanth and SR Krishnadas. Vessel bend-based cup segmentation in retinal images. *In*: Proceedings of the 20th International Conference on Pattern Recognition, Istanbul, Turkey. 2010.